Optical and Quantum Electronics (2023) 55:93
https://doi.org/10.1007/s11082-022-04351-x

Supercontinuum generation in ultra-flattened near-zero dispersion PCF with C_7H_8 infiltration

Thuy Nguyen Thi[1] · Duc Hoang Trong[1] · Lanh Chu Van[2]

Received: 20 May 2022 / Accepted: 1 November 2022

Abstract
A novel design study of ultra-flattened near-zero dispersion PCF with toluene (C_7H_8) infiltration is proposed. The near-zero ultra-flattened dispersion is achieved by appropriately reducing the diameter of the first ring air-holes in the cladding and increasing the distance from the core to these air-holes. An ultra-flattened chromatic dispersion as small as 0.947 ps/(nm.km) has been obtained over a broadband of 500 nm with a high nonlinear coefficient and very low attenuation of the fundamental modes (about 10^{-14} dB/m at the pump wavelength). Two optimized PCFs have been selected for broad-spectrum supercontinuum (SC) generation with low peak power. The first fiber with a lattice constant (Λ) 0.9 μm and filling factor (d_1/Λ) 0.45 has an anomalous dispersion regime. The SC spectrum broadens from 800 to 2800 nm with a full width at half maximum (FWHM) of 1897.3 nm generated by pump pulses centered at a wavelength of 1.55 μm, with input pulse energy of 0.05 nJ and 90 fs duration, corresponding to the peak power of about 0.556 kW. The second proposed fiber ($\Lambda = 1.0$ μm, $d_1/\Lambda = 0.5$) enables SC generation in an all-normal dispersion regime with an FWHM of 1163.7 nm at the same pump pulses as the first fiber with input pulse energy of 0.015 nJ (the peak power of 0.375 kW) in a 5 dB dynamic range. These fibers can be a new class for the next generation of broadband laser sources with a low peak power as cost-effective alternatives to glass core fibers.

Keywords PCF with toluene infiltration · Ultra-flattened near-zero dispersion · All-normal dispersion · Anomalous dispersion · Low attenuation · Low peak power · Supercontinuum generation

✉ Thuy Nguyen Thi
ntthuy@hueuni.edu.vn

✉ Lanh Chu Van
chuvanlanh@vinhuni.edu.vn

[1] University of Education, Hue University, 34 Le Loi, Hue City, Viet Nam

[2] Department of Physics, Vinh University, 182 Le Duan, Vinh City, Viet Nam

Published online: 16 December 2022

1 Introduction

Supercontinuum generation is a huge spectral broadening process occurring while a narrowband optical pulse of high intensity propagates through a highly nonlinear and optically transparent medium (Dudley et al. 2006). Due to its excellent characteristics (large bandwidth, high power density, and good coherence), SC has been widely applied in optical frequency metrology, ultrashort pulse generation, gas sensing, optical telecommunication systems, etc. (Pires et al. 2015; Smirnov et al. 2006; Yoshii et al. 2019; Ling et al. 2013; Hartl et al. 2001; Kaminski et al. 2008; Jones et al. 2000; Shang et al. 2021; Dashtban et al. 2021; Gallazzi et al. 2022; Lemière et al. 2021). Recently, there has been great interest in developing PCF-based SC sources because PCF is considered an excellent nonlinear medium. Specifically, its versatility and flexibility in terms of geometry and background material have led to the easy achievement of the required optical guiding properties (Knight 2003; Thévenaz 2011). The generation of high brightness, good coherence, and broad-spectrum SC is achieved through a synergy between several dispersive and nonlinear effects (Dudley and Taylor 2010). Usually, there are two ways to generate SC involving the anomalous or all-normal dispersion regime of PCF. First, when the pump pulse is operated in the anomalous regime of dispersion, the soliton dynamics, e.g., soliton fission (SF), soliton self-frequency shift (SSFS), and dispersive wave (DW), play a major role in the SC formation (Ferreira 2020). In such a case, although the SC with large bandwidth can be generated, its coherence is low, and the temporal profile is complex and nonuniform. However, these properties can be improved if specific conditions are met, such as the input soliton order, pulse duration, propagation length, etc. (Dudley 2002). Second, when the PCF exhibits an all-normal dispersion regime, the spectrum of output optical pulses is significantly broadened by self-phase modulation (SPM), self-steepening (SS), and optical wave breaking (OWB) mechanisms (Fang et al. 2020). A good coherence, smooth, and flat spectra can be observed by suppresing soliton fission (Finot et al. 2008), but its bandwidth is narrow. In addition, the energy of input laser pulses is injected into the fiber, which is usually much higher than that of the SC generation operating in the anomalous dispersion regime (Dudley et al. 2006).

Thus, the width and flatness of the spectrum over broadband wavelength have been a challenge for researchers in generating quality SC (Dudley et al. 2006). To achieve this, the high nonlinearity and flat chromatic dispersion of PCF are essential. Many works emphasize optimizing the design of the fibers and the pumping condition. In which, optimizing structure to improve the flatness of the dispersion over wider bandwidths has been an attractive approach to achieving high performance in SC generation. In general, there are two suggested different ways for PCFs, the first consists of using additional materials, either by doping the core or the cladding with high index material such as fluorine (Zeleny and Lucki 2013) and germanium (Medvedkov et al. 2012) or by infiltrating high nonlinearity liquids into the core (Van et al. 2019, 2021, 2020; Sharafali et al. 2021; Dinh et al. 2018; Hoang et al. 2020, 2019; Le et al. 2018; Tran et al. 2020). The second way consists only of selectively reducing the radii of the core, air hole, or changing the cladding geometries (Begum et al. 2011; Medjouri et al. 2015; Saitoh et al. 2003, 2006; Stępniewski et al. 2018; Sultana et al. 2018; Islam et al. 2018; Maji and Chaudhuri 2014). Two ways mentioned above can also be reasonably combined to achieve high efficiency in dispersion optimization and broader SC spectra (Van et al. 2020; Tran et al. 2020; Medjouri et al. 2015).

PCFs with ultra-flattened near-zero dispersion have been the efforts of many researchers to generate SC with large bandwidth and high coherence. Many designs for the PCFs have

been proposed to achieve this aim (Medjouri et al. 2015, 2017; Maji and Chaudhuri 2014; Huang et al. 2019, 2021; Huang et al. 2018a, b; Kumar et al. 2020, 2019; Hsu 2016). By appropriately modifying the diameter of the core-neighboring air holes layer, the works (Medjouri et al. 2015; Maji and Chaudhuri 2014) obtained a small, ultra-flattened chromatic dispersion of less than 1.0 ps/(nm.km) over broadband around 400–500 nm. This dispersion property dominated the SC spectrum expansion; FWHM from 400 to 600 nm was achieved with a peak power of a few kW. Recently, the combination of highly nonlinear liquid infiltration into hollow cores or air holes and changing lattice geometry of PCF has been a new design. With a peak power of 3.2 kW, the paper (Medjouri et al. 2017) reported an SC spectrum spanning 700 nm thanks to a nearly zero ultra-flattened chromatic dispersion with air holes of PCF reduced and filled selectively liquid. The ability to generate SC spectrum as broad as 945 nm in the infrared wavelength range based on ultra-flattened all-normal dispersion (1.04 ps/(nm.km)) with ethanol-infiltrated PCF was verified in the work (Le et al. 2018) but unfortunately the peak power was too high, up to 50 kW. Using other substrates to partially or completely replace silica is also new research in improving PCF dispersion. For example, the study (Kumar et al. 2020) achieved a broad SC spectrum up to 2784 nm with a peak power of 5 kW through a PCF with an ethanol-infiltrated lead silicate substrate into the hollow core. Flat dispersion with a value less than 5 ps/(nm.km) is the leading cause of this spectrum's huge broadening. Alternatively, an ultra-flattened normal dispersion within 0.75 ps/(nm.km) generated an SC bandwidth of 238 nm with a relatively high power of 20 kW (Huang et al. 2019). In recent years, the results obtained with ultra-flattened near-zero dispersion PCFs are briefly summarized in Table 1. The obtained results show that the bandwidth SC depends strongly on the ultra-flattened near-zero dispersion of PCFs. Although these previous publications have demonstrated the ability to generate a broad SC spectrum in PCFs with ultra-flattened dispersion, the peak power is still relatively high, from a few kW to several tens of kW. The peak power of the input pulses is also an essential factor in evaluating SC generation performance when using a nonlinear medium such as PCF. Therefore, besides improving dispersion, generating broad-spectrum SC with a low peak power is also the goal of further studies.

In this paper, we present for the first time the possibility of achieving a broad SC spectrum using very low peak power, 0.375 kW excited at 1.55 μm for PCFs with an ultra-flattened near-zero dispersion. We design the circular silica-based PCFs with a C_7H_8-filled core. The diameter of the air holes and lattice constant of the first ring are designed differently from other claddings' rings to optimize dispersion. There are five ideas that guide the design of our PCF structures:

- Silica-based PCFs are very popular because they find advantages in practical fabrication.
- The circular lattice can well confine the electromagnetic field to the core due to its high geometric symmetry i.e. it enhances the fiber nonlinearity, which has not been studied as much as the hexagonal lattice before.
- Again, losing the rings'periodicity near the core is considered to increase the fiber's design freedom to a large extent, because every ring in the structure strongly influences the dispersion. Different air hole rings surrounding the core in PCFs have been designed so far to get better and more engineerable SCs (Ahmad et al. 2020; Lee et al. 2019; Alam et al. 2021; Huang et al. 2018a, b).
- C_7H_8 has a high nonlinear refractive index, relatively low attenuation concerning the other nonlinear liquids, and low toxicity. The nonlinear refractive index of C_7H_8 is $n_2 = 16.8 \times 10^{-19}$ $m^2.W^{-1}$. It is 60 times higher than silica ($n_2 = 2.79 \times 10^{-20}$ $m^2.W^{-1}$)

Table 1 Overview SC generation in several ultra-flattened PCFs

Structures	*D* (ps/(nm.km))	Ultra-flattened dispersion bandwidth (nm)	Pump wavelength (μm)	Dispersion regime	SC range (nm)	Input peak power (kW)	References
Square	0 ± 0.25	510	1.55	Anomalous	450	12	Begum et al. (2011)
Hexagonal	0 ± 0.41	452	1.55	Anomalous	400	4.5	Maji and Chaudhuri (2014)
Circular	± 0.66	400	1.55	Anomalous	600	3.2	Medjouri et al. (2015)
Circular	1.05	300	1.55	Anomalous	600	3.2	Medjouri et al. (2017)
Hexagonal	1.04	500	1.55	Anomalous	945	50	Le et al. (2018)
Hexagonal	1.1	600	2.0	All-normal	238	20	Huang et al. (2019)
Hexagonal lead silicate_ethanol	5.0	About 500	1.55	Anomalous	2784	5.0	Kumar et al. (2020)
Hexagonal PCF3	0 ± 3.345	420	1.05	Anomalous	919	–	Huang et al. (2021)
Hexagonal PCF4	0 ± 4.304	492	1.05	Anomalous	869	–	Huang et al. (2021)

(Kato et al. 1995). This interesting thing of C_7H_8 helps us choose it to fill the hollow core of circular lattice PCF.

- In the experiment, PCFs infiltrated with C_7H_8 can be easily fabricated by the conventional stack-and-draw method (Hoang et al. 2018; Fanjoux et al. 2017). C_7H_8 is filled into the core by integrating a microfluidic pump system using a thermal fusion splicer or laser writing technique (Vieweg et al. 2010). Other applications of toluene-permeable PCF are reported as sagnac interferometer with high sensitivity, and temperature sensors (Mei et al. 2022; Yang et al. 2017).

With such a design, the dispersion characteristic of the PCF can be easily adjusted to achieve all-normal and ultra-flattened near-zero dispersion as small as 0.947 ps/(nm.km) for the wavelength range of 500 nm. SC generation using two optimal fibers with all-normal and anomalous dispersion regimes is numerically demonstrated by solving the generalized nonlinear Schrödinger equation (GNLSE) and using the symmetry split-step Fourier transform method. With a very low peak power of the input pulse (0.375 and 0.556 kW) excited at 1.55 μm for PCFs with all-normal ultra-flattened near-zero dispersion and anomalous dispersion regime, we obtain the broad SC spectrum with an FWHM of 1163.7 nm and 1897.3 nm, respectively.

The paper has four sections. Section 1 introduces an overview of previous studies on PCF-based SC generations. The results with ultra-flattened near-zero dispersion of previous research works have also been discussed in detail. Next, an idea about the design of proposed nonlinear PCF structures with parameters definition is presented in Sect. 2. Then, in Sect. 3, the dispersion and optical properties of the optimal structures (nonlinear coefficient, effective mode area, and attenuation of the fundamental mode) have been discussed based on numerical simulation results. Afterward, Sect. 4 describes how SC can be generated to obtain broad spectra with the low peak power. Lastly, some conclusions have been drawn regarding the proposed PCF structure's effectiveness.

2 Numerical modeling of the PCFs

The cross-section view of the circular C_7H_8-infiltrated PCF (C_7H_8-PCF) is illustrated in Fig. 1a. The cladding consists of eight regularly arranged rings of air holes surrounding the hollow core, which is filled with C_7H_8. We denote Λ as the distance between two adjacent air holes in the cladding, d_1 and d_2 as the diameters of the innermost ring air holes near the core and the others, respectively, which means that the linear filling factor of the innermost and the other rings are defined as d_1/Λ and d_2/Λ. The dispersion control is quite convenient thanks to the diversity in the design of PCFs with various core shapes or different air hole sizes in the cladding (Maji and Chaudhuri 2014). From there, one can quickly achieve ultra-flattened dispersion values over wider bandwidths. Interestingly, the dispersion properties, including flatness and zero-dispersion wavelength (ZDW) shift, are strongly governed by the size of the air holes in the first ring near the core. Meanwhile, the low attenuation of the fundamental mode and even the higher modes are affected by the size of the others rings (Medjouri et al. 2015; Saitoh et al. 2006; Huang et al. 2018a, b). It should be noted that it is difficult to optimize the optical properties of the fiber simultaneously, and dispersion optimization is still preferred in SC generation. To our knowledge, up to now, the difference in lattice constant of the first and other rings of PCF structure is yet to be explored for any possible broad spectra SC generation. Thus, in this simulation, the core

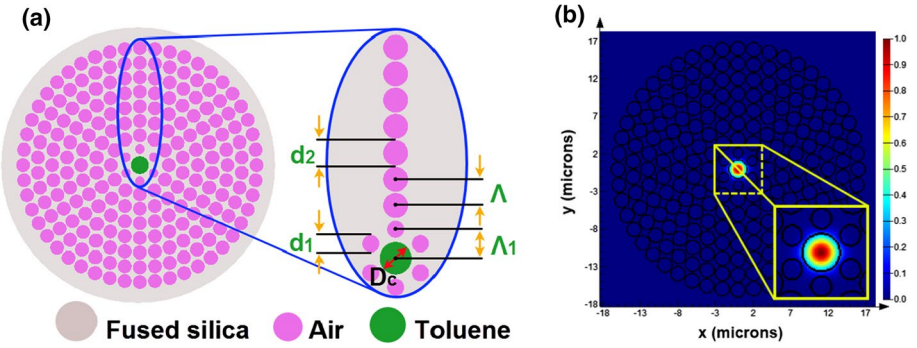

Fig. 1 Cross-section view of the circular C_7H_8-PCF (**a**) and the mode field energy can be well confined in the core region of the C_7H_8-PCF (**b**)

of the designed PCF is liquid-filled, and lattice constant of the rings in the cladding is also appropriately adjusted to achieve the expected optical properties. We keep the same value of 0.95 for the filling factor d_2/Λ but d_1/Λ varies from 0.3 to 0.65. The distance from the core to the air-holes of the first ring is $\Lambda_1 = 1.095\Lambda$ while the distance between the other rings is kept as Λ. We use the following lattice constants Λ: 0.9, 1.0, 1.5 µm, and 2.0 µm. Figure 1b shows that the mode field energy can be well confined in the core region of the C_7H_8-PCF in the wavelength range of 0.6 to 2.0 µm.

Fused silica (SiO_2) is selected as background material in all the designs of these PCFs. Cauchy's equation (Moutzouris et al. 2014) and Sellmeier's equation (Tan 1998) show the dependence of refractive index characteristics on wavelength for C_7H_8 and SiO_2

$$n^2_{C_7H_8}(\lambda) = 2.161659124 + 0.000495188\lambda^2 + \frac{0.021381790}{\lambda^2} + \frac{0.000058838}{\lambda^4} + \frac{0.000087632}{\lambda^6} \tag{1}$$

$$n^2_{SiO_2}(\lambda) = 1 + \frac{0.6961663\lambda^2}{\lambda^2 - (0.0684043)^2} + \frac{0.4079426\lambda^2}{\lambda^2 - (0.1162414)^2} + \frac{0.8974794\lambda^2}{\lambda^2 - (9.896161)^2} \tag{2}$$

where λ is the excitation wavelength in micrometers, $n(\lambda)$ is the wavelength-dependent linear refractive index of materials.

The refractive indices of toluene and silica are shown in Fig. 2a. Toluene has a refractive index higher than silica, thus the light is guided in the core by total inter refraction, and confinement loss is neglected in our model. We also assumed that fiber losses are only contribution from material loss of toluene, as shown in Fig. 2b. Thus, the fibers have a high loss in long wavelengths (i.e., $\lambda > 1.6$ µm) as shown in Fig. 7.

The Lumerical Mode Solutions (LMS) with the full-vector finite-difference eigenmode (FDE) method has been used to create C_7H_8-filled PCF and achieve the field intensity profile of the fundamental mode of the PCFs. In order to design the structure of the hollow-core PCF filled with C_7H_8, the refractive index and attenuation data of C_7H_8 must be correctly and carefully put in the LMS materials database. Among the recommended geometric structure of the data system, we choose the hollow-core circular lattice, while the SiO_2 base material is created in the structure. Then the C_7H_8 is put into the hollow-core of the designed PCFs. PCFs infiltrated with C_7H_8 can be experimentally fabricated easily by the conventional stack-and-draw method. Some techniques, such as integrating a microfluidic pump system using a thermal fusion splicer or laser writing technique, enable C_7H_8 to

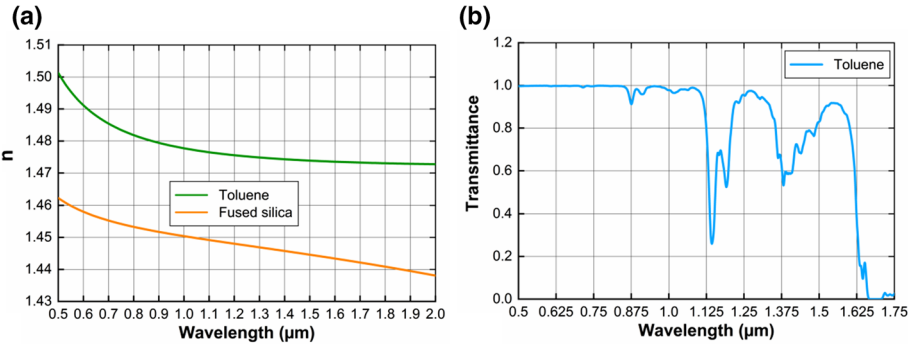

Fig. 2 Real parts of refractive index of toluene and fused silica (**a**) and transmittance of 1 cm toluene sample (**b**) (Kedenburg et al. 2012)

be filled into the hollow core accurately and efficiently (Hoang et al. 2019). For SiO_2, reliable data are only available in the wavelength range of 0.6–2.0 μm, so we limit the simulation to this range. The characteristic properties of C_7H_8-filled PCF are simulated assuming that C_7H_8 exhibits significant losses. The process of FDE utilizes the Maxwell wave equation and the boundary condition for simulation is a perfectly matched layer, allowing no reflection at the boundary and reducing the loss.

3 Optical properties of the PCFs

Higher order modes have no significant effect on the SC broadening if the input pulse is sufficiently short (≤ 10 ps), so here we only present the fibers' dispersion and nonlinear properties in the fundamental mode. The chromatic dispersion which depends on both material dispersion (D_M) and waveguide dispersion (D_W) can be obtained by (Lee et al. 2019):

$$D_C = D_W + D_M = -\frac{2\pi c}{\lambda^2}\beta_2 \tag{3}$$

where c is the velocity of light in a vacuum and β_2 is the second-order dispersion, usually called the group velocity dispersion (GVD). The GVD is responsible for the determination of the range up to which the spectral components of an ultra-short pulse propagate in the PCF structure at different phase velocities (Dudley et al. 2006; Agrawal 2013). Here, D can be directly calculated by

$$D = -\frac{\lambda}{c}\frac{\partial^2 \mathrm{Re}[n_{\mathrm{eff}}]}{\partial \lambda^2} \tag{4}$$

where $\mathrm{Re}[n_{\mathrm{eff}}]$ is the real part of the effective index of the guided mode.

The dispersion regime of C_7H_8-filled PCFs is depicted in Fig. 3a, b, c, and d, respectively. Obviously, the difference in the filling factor d_1/Λ in the first cladding ring and the lattice constants Λ are responsible for the rather diverse variation of the dispersion properties. We achieve both all-normal and anomalous dispersion regimes over the investigated wavelength range for PCFs with small lattice constants ($\Lambda = 0.9$ μm and 1.0 μm). As Λ increases ($\Lambda = 1.5$ μm and 2.0 μm), the anomalous dispersion regime with one

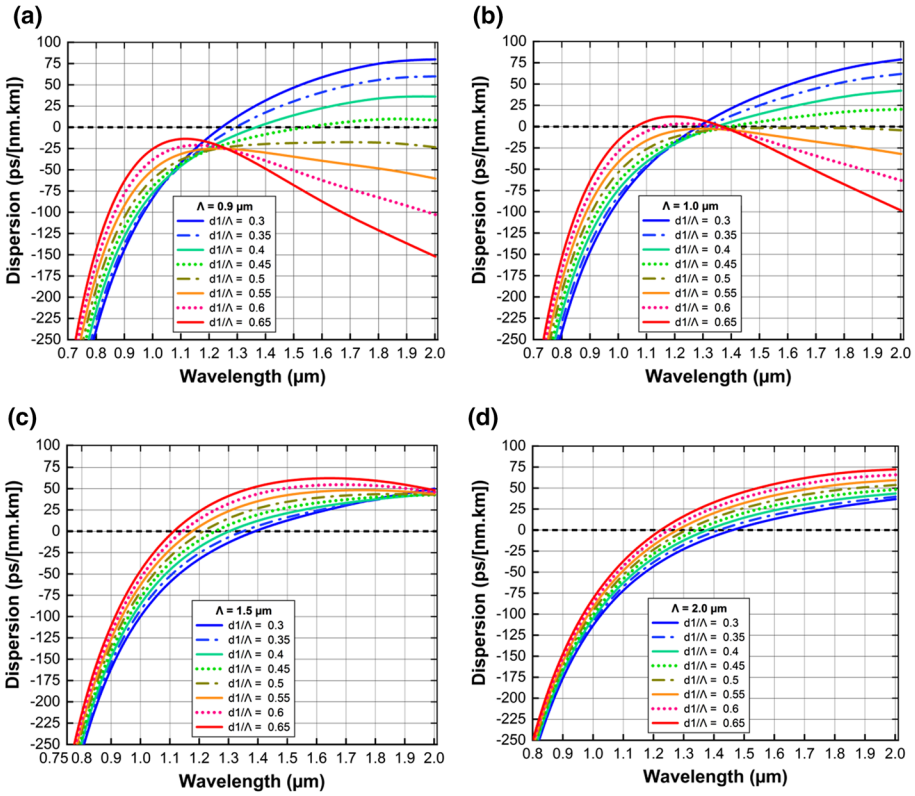

Fig. 3 The dispersion characteristics of C_7H_8-PCFs with various values of d_1/Λ and $\Lambda = 0.9$ μm (**a**); 1.0 μm (**b**); 1.5 μm (**c**); 2.0 μm (**d**)

ZDW dominates completely. For $\Lambda = 0.9$ μm (Fig. 3a), four all-normal dispersion curves are found with $d_1/\Lambda \geq 0.5$ while anomalous dispersions with one ZDW are obtained with d_1/Λ is smaller (from 0.3 to 0.45). As the filling factor d_1/Λ is reduced (from 0.65 to 0.5), the all-normal dispersion curves get closer and closer to the zero dispersion and become flatter. In this case, PCF with $d_1/\Lambda = 0.5$ has the flattest all-normal dispersion curve and is closest to zero dispersion. More interestingly, when $\Lambda = 1.0$ μm (Fig. 3b) the curves with $d_1/\Lambda \leq 0.45$ still exhibit the anomalous dispersion properties with one ZDW similar to the case $\Lambda = 0.9$ μm. Meanwhile, two dispersion curves with $d_1/\Lambda = 0.6$ and 0.65 intersect the horizontal axis at two points respectively i.e. there are two anomalous dispersion curves with two ZDWs. Thus, we get two all-normal dispersions for $d_1/\Lambda = 0.5$ and 0.55 in the case $\Lambda = 1.0$ μm.. In particular, we achieve the near-zero ultra-flattened dispersion as small as 0.947 ps/(nm.km) over a broadband of 500 nm with all-normal dispersion when $d_1/\Lambda = 0.5$. It is clear from Fig. 3a and b that the dispersion characteristic can be tuned easily with air hole diameter d_1 in the first ring of the PCF structure. Figure 3a and 3b also expose that the dispersion slope changes drastically for a variation of d_1. The interaction between waveguide dispersion and material dispersion could explain this change. For smaller d_1/Λ, material dispersion plays a major role while the waveguide effect dominates for higher d_1/Λ (Maji and Chaudhuri 2014). When

Table 2 The values of ZDW of C_7H_8-core PCFs with various values of d_1/Λ and Λ

d_1/Λ	$\Lambda = 0.9$ μm	$\Lambda = 1.0$ μm		$\Lambda = 1.5$ μm	$\Lambda = 2.0$ μm
	$ZDWs_1$	$ZDWs_1$	$ZDWs_2$	ZDWs	ZDWs
0.3	1.243	1.283	–	1.389	1.459
0.35	1.292	1.313	–	1.348	1.415
0.4	1.364	1.347	–	1.3	1.375
0.45	1.54	1.392	–	1.253	1.34
0.5	–	–	–	1.213	1.307
0.55	–	–	–	1.175	1.278
0.6	–	1.145	1.34	1.142	1.249
0.65	–	1.062	1.372	1.113	1.223

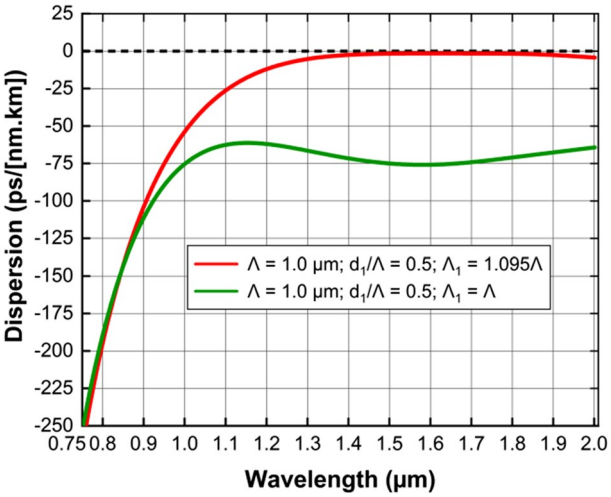

Fig. 4 Dispersion characteristic of two structures with the difference in the distance from the core to air-holes of the first ring

$\Lambda = 1.5$, and 2.0 μm, the decrease of the filling factor reduces the dispersion without much change in slope, and PCFs exhibit anomalous dispersion regimes with a larger shift of ZDWs towards the longer wavelength region. Because of the predominance of material dispersion, the increase of Λ (while keeping the filling factor fixed) also causes the ZDW to shift towards the longer wavelength, the values of ZDW are presented in Table 2. Shifting the ZDW toward the longer wavelengths in PCFs plays an important role for soliton-driven SC by low cost and short pulse lasers with the pump wavelength chosen to be larger but closer to ZDW. For $\Lambda = 0.9$ μm and $d_1/\Lambda = 0.45$, the value of ZDW is 1.54 μm, which is very approximate to the common pump wavelength in SC generation based silica-PCF.

To obtain the near-zero ultra-flattened dispersion in PCF infiltrated with C_7H_8, we optimized the structural parameters of Λ and Λ_1. In optimizing parameter Λ_1, the distance from the core to air-holes of the first ring plays a crucial role in controlling the flatness of dispersion over the broadband region. With little modification in distance Λ_1, $\Lambda_1 = 1.095\Lambda$, a great influence is observed in the dispersion characteristic of PCF. This is illustrated in Fig. 4 with the dispersion properties of two structures, $\Lambda = 1.0$ μm, $\Lambda_1 = 1.095\Lambda$, $d_1/\Lambda = 0.5$ (red line), and $\Lambda = 1.0$ μm, $\Lambda_1 = \Lambda$, $d_1/\Lambda = 0.5$ (green line). In our study, by careful choice of the

structural parameter Λ_1, we can control and obtain the desired dispersion characteristic of C_7H_8-filled PCF.

The chromatic dispersion causes a change in the optical pulse per unit distance of the propagation length of the fiber, so a PCF with suitable dispersion characteristics has been an important factor governing the efficiency of SC generation. Usually, the PCF has an all-normal and flat dispersion necessary for expansion spectrum in SC generation in the visible and near-infrared regions to get a good coherence, smooth, and flat spectra. Meanwhile, low anomalous dispersion near the ZDW generates a broad supercontinuum with strong confinement to the core despite low input energy. Moreover, the ultra-flattened dispersion and the shift of the ZDW to the longer wavelength are favorable conditions for using an available laser with femtosecond optical pulses as input sources for wider bandwidth supercontinuum generation (Raei et al. 2018). Based on the above investigations, we select two optimal PCFs to benefit the generation SC, called $\#F_1$ and $\#F_2$. Both structures give reasonable flatness dispersion and near-zero dispersion in the investigated wavelength region, displayed in Fig. 5. The first fiber $\#F_1$, with $\Lambda = 0.9$ µm, and $d_1/\Lambda = 0.45$, has the anomalous regime of dispersion which is used for SC generation at 1.55 µm the pump wavelength. While the second fiber $\#F_2$ ($\Lambda = 1.0$ µm and $d_1/\Lambda = 0.5$) operates in an all-normal dispersion regime with near-zero ultra-flattened dispersion, which is expected to generate a smooth and broad-spectrum SC at the same pump wavelength of $\#F_1$ fiber. Both $\#F_1$ and $\#F_2$ have low dispersion at the pump wavelength, are 0.489 and –1.534 ps/(nm.km) respectively. Note that the PCF's core diameter also strongly influences the SC generation because the large core will increase the effective mode area and ultimately reduce the nonlinear coefficient. The core diameters of these PCFs are determined by the formula $D_c = 2\Lambda - 1.2d_1$, two proposed fibers have small cores and low dispersion at the pump wavelength (Table 3) that are expected to be favorable for SC generation.

The interaction of the input pulse with the nonlinear optical medium through various nonlinear phenomena such as SPM, cross-phase modulation (XPM), stimulated Raman scattering (SRS), DW, FWM,… results in a broad SC spectrum. So, the nonlinear properties of an optical medium contribute to generating new frequencies (Alam et al. 2021). The nonlinear coefficient (γ) is a measure of the nonlinearity of the medium and it can be estimated by the formula (Agrawal 2013).

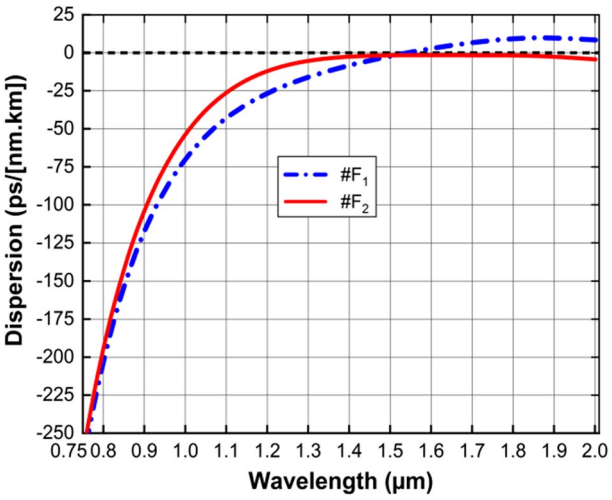

Fig. 5 The dispersion characteristics of the fundamental mode for the $\#F_1$ and $\#F_2$ optimal fiber

Table 3 The structure parameters and the characteristic quantities of proposed PCFs at the pump wavelength compared with other publications on C_7H_8-infiltrated PCFs

#	D_c (μm)	Λ (μm)	d_1/Λ	A_{eff} (μm^2)	γ (W^{-1}.km^{-1})	D (ps/(nm.km))
#F_1	1.314	0.9	0.45	2.527	2699.919	0.489
#F_2	1.4	1.0	0.5	2.632	2592.282	−1.534
#F_1 (Thi et al. 2022)	1.16	1.0	0.7	1.221	7827.614	−0.557
#F_2 (Thi et al. 2022)	4.64	2.5	0.3	10.497	899.836	1.502
#I_0.3 (Van et al. 2017)	3.28	2.0	0.3	7.79	2132.575	−7.784
#I_0.35 (Van et al. 2017)	2.8	2.0	0.5	78.9	2890.276	−1.19

$$\gamma(\lambda) = 2\pi \frac{n_2}{\lambda A_{\text{eff}}} \tag{5}$$

where A_{eff} is the area of the effective mode for the basic mode of the fiber and n_2 is the nonlinear refractive index of the optical material. The effective mode area for the fundamental mode can be calculated by using (Raei et al. 2018).

$$A_{\text{eff}} = \frac{\left(\int_{-\infty}^{\infty}\int_{-\infty}^{\infty} |E|^2 dxdy\right)^2}{\int_{-\infty}^{\infty}\int_{-\infty}^{\infty} |E|^4 dxdy} \tag{6}$$

where E is the transverse electric field over the cross-section of the PCF.

The variation of the nonlinear coefficient and the effective mode area as functions of wavelength have been shown in Fig. 6. The nonlinear coefficient is inversely proportional to the effective mode area, so for both #F_1 and #F_2, increasing the effective mode area with wavelength reduces the nonlinear coefficient. The small effective mode area and high nonlinear coefficient are beneficial factors for SC generation, but in the long wavelength region, the effective mode area has a large value. The light is not well confined in the core leading to leakage of modes to the cladding, which is the cause of

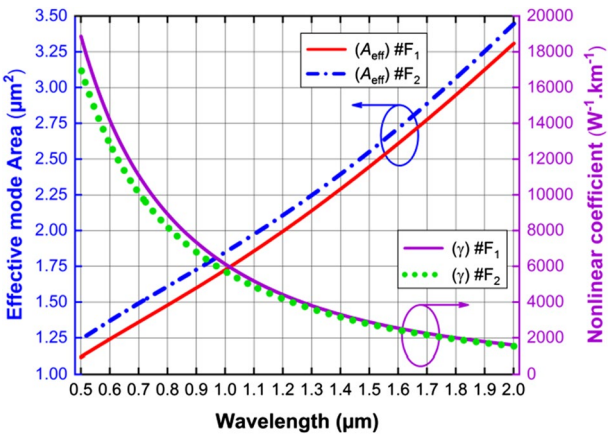

Fig. 6 The effective mode area and nonlinear coefficient of the fundamental mode for #F_1 and #F_2 fiber

the increase in effective mode area as the wavelength increases. Furthermore, the small cores often exhibit better light confinement efficiency than large cores, so $\#F_1$ fiber has a smaller effective mode area than $\#F_2$ fiber in the investigated wavelength range. However, the difference in effective mode area at 1.55 μm pumps wavelength of the two optimal fibers is not large, equal to 0.105 μm^2. The limit of core diameter increase is also a factor to keep in mind when simulating the optical properties of PCF because the higher-order modes will appear in the fiber core if the effective mode area is too large. This will not benefit the SC generation. With the same pump wavelength of 1.55 μm, the effective mode area of the fundamental mode of fibers $\#F_1$ and $\#F_2$ are 2.527 μm^2 and 2.632 μm^2, respectively. These values are much smaller in comparison with previous publications of PCF with C_7H_8 infiltration (Hoang et al. 2018; Thi et al. 2022; Van et al. 2017). As expected, the nonlinear coefficients of $\#F_1$ and $\#F_2$ are relatively high, 2699.919 $W^{-1}.km^{-1}$ and 2592.282 $W^{-1}.km^{-1}$, respectively. The small dispersion and high nonlinear coefficients will be favorable conditions for the broad SC spectrum with low peak power.

Loss of the proposed fibers are shown in Fig. 7. In our model, the confinement losses are neglected, and only material losses of toluene contribute to the fiber losses. The fibers have a low loss in the visible range. However, it exponentially increases in the long wavelength range, and the peak is up to 600 dB/m at $\lambda = 1.68$ μm. We did not character the loss for further long wavelength ($\lambda > 1.75$ μm) because of the lack of reliable data in the state-of-the-art and limitation of the versatile wavelength range of available spectrometer in our lab. Therefore, in our model, we assume that the fiber losses in the long wavelength range have a value of 600 dB/m (equal to the peak value).

The losses of fibers are taken into account in our model for the simulation of SC generation. Notwithstanding, the effect of fiber losses is not visible in the spectral broadening because the high nonlinear refractive index of toluene enables to broad bandwidth of the SC spectrum induced in a short propagation (a few centimeters). For instance, a 10 cm fiber sample of the proposed fibers is used for octave spanning SC generation with low peak power of input pulses.

Table 3 shows the structural parameters and the characteristic quantities of the two proposed PCFs at the pump wavelength compared with other publications on C_7H_8-infiltrated PCFs (Thi et al. 2022; Van et al. 2017).

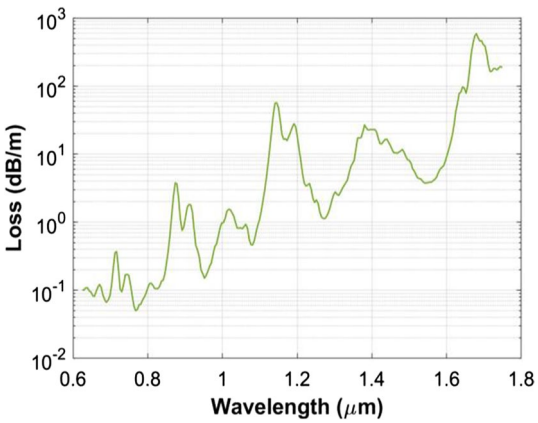

Fig. 7 The loss of the proposed fibers

4 Supercontinuum generation in proposed fiber

The higher-order dispersions are calculated through the development coefficients of the Taylor series around the center wavelength ω_0, and the expansion of the propagation constant (β) can be obtained by (Agrawal 2013).

$$\beta(\omega) = \beta(\omega_0) + \beta_1(\omega_0)(\omega - \omega_0) + \frac{1}{2!}\beta_2(\omega_0)(\omega - \omega_0)^2 + \tag{7}$$

Then the nth order dispersion term can be calculated by taking the derivative of β concerning the angular frequency ω (Raei et al. 2018). Thus

$$\beta_n = \left.\frac{d^n\beta}{d\omega^n}\right|_{\omega=\omega_0} \tag{8}$$

In our numerical modeling, the high-order dispersions at the pumping pulse frequency are shown in Table 4.

The analyzed chromatic dispersion and nonlinear properties above exhibit the large potential to generate SC for the proposed C_7H_8-filled PCFs. The refractive index of the medium is changed drastically due to the infiltration of C_7H_8 into the core and the flexibility in structural design, which leads to the nonlinear effects in SC generation. The propagation of pump pulses in a nonlinear medium such as PCF can be described by the Schrödinger equation (GNLSE) which is given by the Eq. 9 (Dudley and Taylor 2010):

$$\partial_z\tilde{A} - i\tilde{\beta}(\omega)\tilde{A} - \frac{\tilde{\alpha}(\omega)}{2}\tilde{A} = i\gamma\left(1 + \frac{\omega - \omega_0}{\omega_0}\right)\tilde{A}F\left[\int_{-\infty}^{\infty} R(T')|A|^2(T - T')dT'\right] \tag{9}$$

where $A(z,\ \omega)$ is Fourier transform of the amplitude of a pulse $A(z,\ T)$, and $R(T')$ is the Raman response function. The left side of Eq. (9) depicts the linear propagation effects of the fiber, $\tilde{\alpha}$ and $\tilde{\beta}$ are attenuation and dispersion in the frequency domain, respectively.

The response function $R(T')$ depends on nonlinear mechanisms original from bound-electron and molecular, such as molecular reorientation, molecular interactions, collision-induced polarizability, and electronic response. Formula of $R(T')$ is written in Eq. 10 (Hoang et al. 2018).

Table 4 The coefficient of high order dispersion at the pump wavelength

Coefficients	#F_1	#F_2
β_2 (ps^2/m)	-5.7×10^{-4}	2×10^{-3}
β_3 (ps^3/m)	8.42×10^{-5}	-1.88×10^{-6}
β_4 (ps^4/m)	-2.64×10^{-7}	1.59×10^{-7}
β_5 (ps^5/m)	-3.49×10^{-10}	3.03×10^{-10}
β_6 (ps^6/m)	4.56×10^{-11}	-6.35×10^{-11}
β_7 (ps^7/m)	-2.58×10^{-13}	9.31×10^{-13}
β_8 (ps^8/m)	-7.09×10^{-15}	3.22×10^{-14}
β_9 (ps^9/m)	-2.30×10^{-17}	-1.17×10^{-15}
β_{10} (ps^{10}/m)	5.06×10^{-18}	2.37×10^{-18}
β_{11} (ps^{11}/m)	-5.65×10^{-20}	5.74×10^{-19}

$$R(T') = \left[2n_{el} + \left(n_{2l} C_{2l} e^{-T'/t_{fl}} \int_0^{\infty} \frac{\sin(\omega T')}{\omega} g(\omega) d\omega + \sum_{k=c,d} n_{2k} C_{2k} \left(1 - e^{-T'/t_{rk}}\right) e^{-T'/t_{fk}} \right) \Theta(T') \right] \frac{1}{N} \tag{10}$$

In which, the subscripts *el, d, l, c* indicate the bound-electronic, molecular reorientation, molecular interaction, and collision-induced, respectively, the coefficient $C_{2l,2d,2c}$ are normalized constant and $N=(n_{2el}+n_{2c}+n_{2d}+n_{2l})$. g(ω) is the distribution function of librational motion as given in Eq. 11.

$$g(\omega) = e^{\left(-\frac{(\omega-\omega_0)^3}{2\sigma^2}\right)} - e^{\left(-\frac{(\omega+\omega_0)^3}{2\sigma^2}\right)} \tag{11}$$

In which, ω_0 and σ are are the center frequency and bandwidth, respectively. In the response function *R(t')* we assumed that $n_{2el}=0.6\times10^{-19}$ m^2.W^{-1}, $n_{2d}=3\times10^{-19}$ m^2.W^{-1}, $\tau_{r,d}=0.25$ ps, $\tau_{f,d}=2.1$ ps, $n_{2l}=1.2\times10^{-19}$ m^2.W^{-1}, $n_{2c}=0.12\times10^{-19}$ m^2.W^{-1}, $\tau_{r,c}=0.25$ ps, $\tau_{f,d}=0.2$ ps, $\omega_0=11$ ps^{-1}, $\sigma=8$ ps^{-1} (Hoang et al. 2018).

The symmetry split-step Fourier transform method is used to solve Eq. (9). In this context, the total path of the pulse propagation in the fiber is divided into very short sections with a length of 2×10^{-4} m. The time window is 22 ps divided into $N=2^{13}$ sections (i.e., the time resolution of 2.7 fs, or 0.2856 THz).

We have carried out our numerical calculations for the proposed fibers with short lengths of 10 cm and 1 cm, the broad spectra generated with low peak power strongly depends on the anomalous and all-normal dispersion regime. Regarding the thermal properties of the proposed optical fibers, further enhancing the pump power is a consideration during SC generation. The higher energy for the longer times can lead to the burning of toluene (Hoang et al. 2018). Although the two optimal fibers exhibit different dispersion properties, the pump wavelengths were chosen at 1.55 µm, which is close to the maximum point of the dispersion curve to obtain the minimum dispersion value beneficial to the SC process. Normally, SC generation with anomalous dispersion PCFs requires a higher peak power than all-normal dispersion PCFs and its SC spectrum is also broader.

Figure 8 illustrates the evolution of the simulated SC over a propagation distance of 10 cm of #F_1 fiber length. A narrow incident pulse of 90 fs duration is pumped at the wavelength of 1.55 µm with an input pulse energy varying from 0.001 nJ to 0.05 nJ corresponding to a peak power from 0.011 kW to 0.556 kW in the 5 dB dynamic range caused the SC spectrum to expand and the SC bandwidth to increase with the increase of peak power. The SC spectrum expansion for fibers with anomalous dispersion regime is explained based on soliton dynamics with typical effects such as SF, SSFS and DW (Dudley et al. 2006). It is difficult to find the symmetry of the SC spectrum in this case because of the existence of solitons. We observe that the spectrum is more broadened towards the redshifted wavelengths and restricted on the opposite side i.e. blueshifted wavelength. The Raman soliton self-frequency shift pushes the soliton components to shift towards the low-frequency as the solitons travel at a further propagation distance which causes the spectrum to widen towards the red side. Meanwhile, the influence of high-slope dispersion at high frequencies is the reason for the limitation of spectral expansion on the blue side. On the other hand, when the input pulse energy is large, the DW components generated from the four-wave mixing (FWM) process also contribute to the limitation of SC spectrum expansion because they propagate without any frequency shift (Van et al. 2021; Alam et al. 2021).

The SC spectral bandwidth increases with the input pulses' energy indicated in Fig. 8a. We observe that most of the SC spectrum is noisy, which is commonly occurred

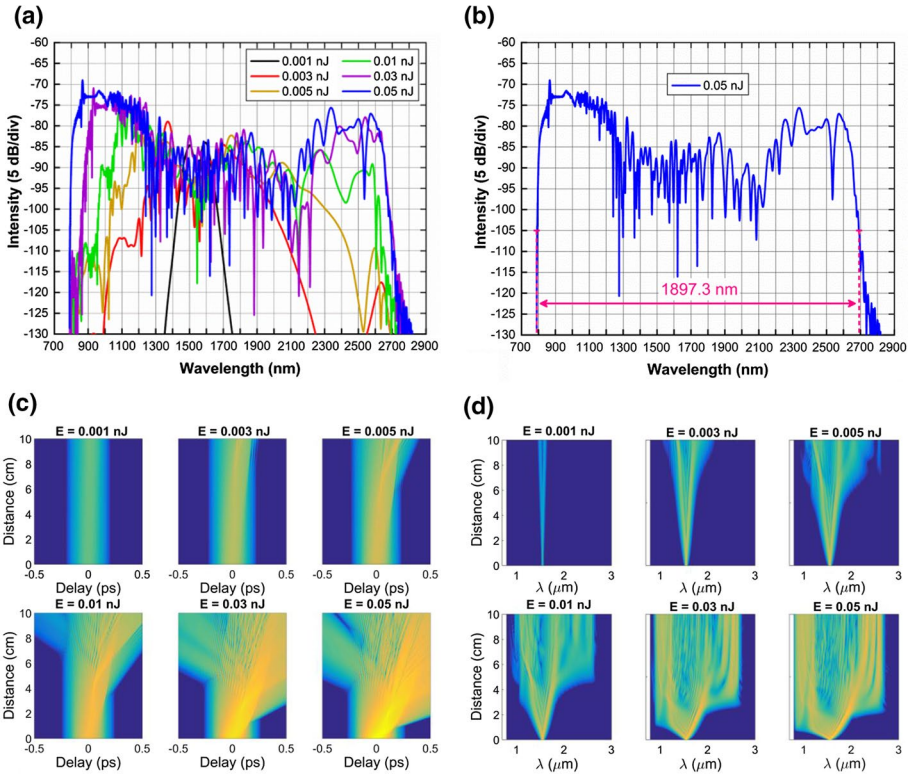

Fig. 8 For #F_1 fiber: **a** the output spectrum for various input pulse energies when using pump pulses with 1.55 μm pump wavelength and 90 fs duration, **b** the output spectrum with the input pulse energy of 0.05 nJ, **c** the temporal profile versus propagation length at various input pulse energies, and **d** the pulse evolution of the SC along with fiber

when generating SC with an anomalous dispersion regime of PCFs. The symmetry of the SC spectrum and the small bandwidth are two typical features for the main dominance of the SPM effect when the input pulse energy is low, 0.001 nJ corresponding to 0.011 kW of peak power. Obviously the peak power of the input pulse is not high enough for the soliton to appear in this case. As the peak power rises, the symmetry of the spectrum disappears. Instead, the right side of the spectrum shifts gradually towards the red wavelength and the spectral width becomes larger. The SF occurs at an input pulse energy of 0.003 nJ (about 0.033 kW) and continues to influence the spectral expansion as the peak power is further increased. But unfortunately, we find that the spectrum width does not increase anymore when the input pulse energies are 0.03 nJ (the peak power is about 0.33 kW) and 0.05 nJ (about 0.556 kW). For these two cases, the bandwidth difference is not large, even the spectrum on the red-side almost coincides. The reason for this limitation of spectral broadening is the high steep dispersion in the short-wavelengths and large effective mode area in the long-wavelength of #F_1 fiber. When the peak power increases to the maximum value of 0.556 kW, SC generation has the broadest spectrum spanning from 800 to 2800 nm with an FWHM of 1897.3 nm (Fig. 8b).

Figure 8c and d show the temporal profile at various propagation lengths and the pulse evolution of the SC along with the fiber. With a peak power of about 0.556 kW (corresponding to the input pulse energy of 0.05 nJ), the SC spectrum is symmetrically broadened within a few millimeters of the initial propagation due to the SPM effect. Since pump wavelength (1.55 μm) is close to the ZDW (1.54 μm), a fraction of the spectrum is induced by SPM across the ZDW and experienced in the normal dispersion regime before soliton fission occurs. A new wavelength band around 0.8 μm is generated by the FWM at a propagation distance of about 5 mm. The spectrum broadens towards the blue-side, which is attributed to OWB due to the interference of the SPM-induced spectrum's trailing with the pulse tail (Van et al. 2022). The soliton fission appears at 2 cm of propagation length, a high-order soliton begins to split into a series of fundamental solitons owing to higher-order dispersion and Raman scattering (Dudley et al. 2006; Dudley and Taylor 2010). The soliton spectrum is shifted towards the red-side causing the bandwidth to expand from 800 to 2800 nm. However, the spectrum will be more difficult to expand if the peak power continues to increase because of longer wavelengths moving more slowly in the anomalous dispersion region (Roy et al. 2010) and the large effective mode area on the long-wavelength side.

#F_2 fiber with all-normal near-zero ultra-flattened dispersion will meet the requirement to generate a flat and wide SC spectrum with low peak power. SPM followed by OBW are the main nonlinear effects that help us to explain the SC spectral broadening when the fiber is pumped in an all-normal dispersion regime. With a pump wavelength of 1.55 μm, a duration of 40 fs, a narrow pulse propagating in 1 cm of the #F_2 fiber length, interacting with the nonlinear medium, causes the SC spectrum to broaden. The relationship between the SC spectrum widths and the input pulse energy was set up in the range 0.001–0.015 nJ, corresponding to the peak power from 0.025 to 0.375 kW displayed in Fig. 9a. The simulation results show that the spectral width will increase with an increase in peak power. With a low peak power of 0.011 kW and 0.075 kW (for 0.001 nJ and 0.003 nJ input pulse energies, respectively), the output pulse is symmetric because only the SPM effect occurs. The spectral expansion in this case is also limited. As soon as the peak power is further increased, the symmetry of the SC spectrum is gone. The SPM effect only dominates the spectral broadening around the central wavelength at a few millimeters of the propagation length. Then the spectrum is broadened in the wings due to OWB through the FWM effect at a longer propagation distance. In the case of the peak power of 0.15 kW (0.006 nJ of input pulse energy), the OWB begins to show its influence at a wavelength of 1.1 μm. This effect occurs at a shorter wavelength with the further increase of the input pulse energy. When the peak power reaches the maximum value of 0.375 kW, which corresponds to 0.015 nJ input pulse energy, the SC spectrum spans the wavelength range of 800–2100 nm with an FWHM of 1163.7 nm (Fig. 9b).

Figure 9c and d present the temporal profile at various propagation lengths, and the pulse evolution of the SC along with the fiber. In the case of peak power of 0.375 nJ, the spectrum has been symmetrically broadened when propagating a very short distance from the initial propagation length because of the main contribution of SPM. The blue-shifted (trailing) edge and the red-shifted (leading) edge of the pulse are observed in Fig. 9d, which is typical for the main influence of the OWB effect and the spectrum broadens asymmetrically toward shorter and longer wavelengths. At a propagation length of about 4 mm, OWB occurs at the trailing edge of the pulse and the newly generated wavelengths appear around 0.8 μm. This is due to the following reasons: ''the SPM-induced spectrum experiences effects of the dispersion in further propagation, and the new short-wavelengths generated by SPM at the trailing edge travel slower than the pulse tail at the center of the

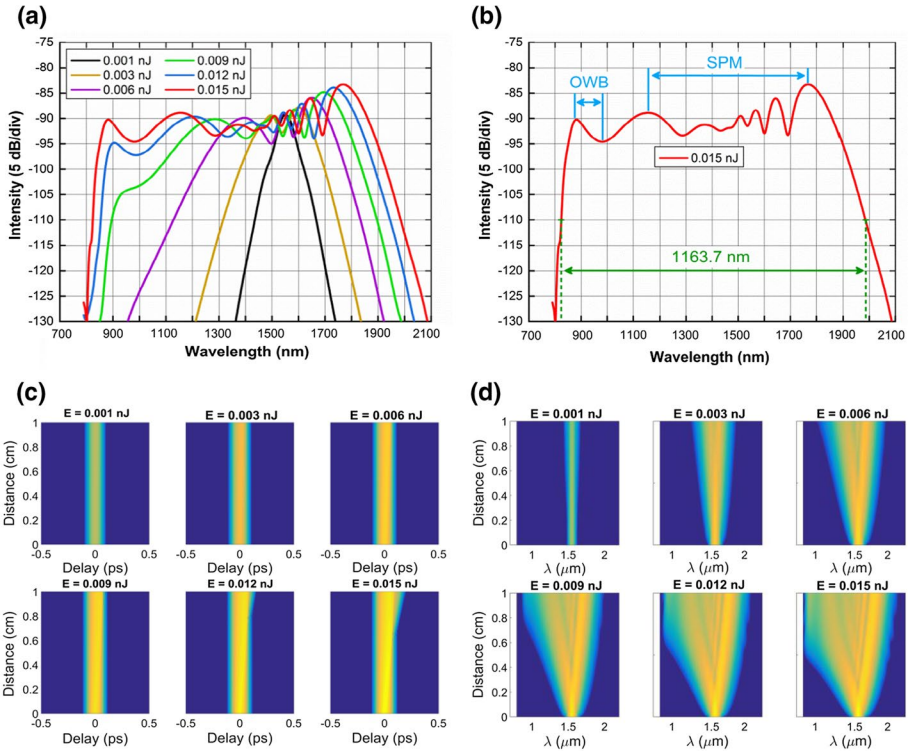

Fig. 9 For #F_2 fiber: **a** the output spectrum for various input pulse energies when using pump pulses with 1.55 μm pump wavelength and 40 fs duration, **b** the output spectrum with the input pulse energy of 0.015 nJ, **c** the temporal profile versus propagation length at various input pulse energies, and **d** the pulse evolution of the SC along the fiber

pulse. The interference of the pulse tail and the slower wavelengths leads to the onset of OWB, and the new wavelengths can be created via four-wave mixing (FWM)'' (Van et al. 2019; Hoang et al. 2019). However, the spectral expansion on the short wavelength side is limited by the high slope of the dispersion (Van et al. 2022). At the same time, the low nonlinear coefficient and high loss in the long-wavelength range of the #F_2 fiber make the spectrum not extend further in this side. We achieve the broadest SC spectrum covering 800 nm to 2100 μm of the wavelength within the 5 dB dynamic range. With the proposed #F_2 fiber, the wavelength range of the generated SC is significantly wider than that in the work (Hoang et al. 2018; Thi et al. 2022; Van et al. 2017) due to the combined effect of SPM and near-zero ultra-flattened dispersion. Additionally, the length of PCF is enormously small, thereby reducing the propagation losses (Maji and Chaudhuri 2014).

The simulation parameters for two fibers #F_1 and #F_2 are typical for several fiber femtosecond lasers reported previously (Sobon et al. 2016). The spectral evolution in Figs. 8c and 9c shows that the spectral expansion in the propagation length depends on the attenuation of toluene. For fibers with all-normal dispersion (in case of maximum input energy), the continuum is fully broadened from 1.1 to 1.75 μm. It flattens after 4 mm of fiber length and its intensity increases slightly until 1 cm of the fiber length (Fig. 8c). As the pulse propagates further, the high loss of the fiber dominates. The spectrum should begin

to truncate at the toluene absorption wavelength but the spectrum broadens to 2100 nm towards the red-side thanks to ultra-flat near zero dispersion of fiber. The short fiber length of 1 cm is an advantage for spectral shaping after SC generation occurs within the first few millimeters of the fiber (Van et al. 2017). With the anomalous dispersion mode, the resulting spectrum is no longer flat (Fig. 9c). However, the spectrum extends to 2800 nm towards the red-side due to the fiber's advantages such as small flat dispersion and high nonlinear coefficient. At a very short propagation distance, only a few millimeters of fiber length, SC generation occurs fastly due to the low attenuation and high nonlinearity of toluene, the spectrum is shaped after about 2 cm of propagation and extended until 10 cm length of the fiber.

Thus, the choice of fiber length in the SC generation is an essential factor in PCF fabrication because it is related to the attenuation of liquids infiltrated into the hollow core of the PCFs. The proposed fibers with assumed length greater than 10 cm were not investigated in this work. The cost of manufacturing PCFs is in fact quite expensive, so short fiber lengths are more favorable.

5 Conclusion

In this work, we reported the numerical simulation for SC generation in C_7H_8-filled core PCF with the femtosecond lasers as the pump sources. With the modification of structure parameters, the distance from the core to air-holes of the first ring is suitably adjusted to achieve a near-zero ultra-flattened dispersion, as small as 0.947 ps/(nm.km) is obtained over a broadband of 500 nm. The fibers also have a smaller and flatter dispersion than those with liquids infiltration in previous works (Hoang et al. 2020, 2019, 2018; Van et al. 2021, 2020, 2017; Tran et al. 2020; Thi et al. 2022). Thus, they enable broad SC generation with low peak power. From the preliminary fiber design, we selected two fibers with optimized dispersion characteristics and analyzed SC generation in each when pumped with pulses having a 1.55 µm central wavelength, 40 and 90 fs duration, respectively.

#F_1 fiber, with lattice constant $\Lambda = 0.9$ µm and filling factor $d_1/\Lambda = 0.45$ has the anomalous dispersion regime. In this fiber, SC is mainly induced by soliton dynamics spanning the range of 700 to 2800 nm with low input pulse energy of 0.05 nJ corresponding to the peak power of about 0.556 kW.

#F_2 fiber, with $\Lambda = 0.9$ and $d_1/\Lambda = 0.5$, exhibits all-normal dispersion regime. With input pulse energy of 0.015 nJ (the peak power of 0.375 kW), #F_2 fiber offers the flat and broad SC with a spectral bandwidth of 800–2100 nm within 5 dB. The SC generation is induced by SPM at the center of the spectrum and OWB at the spectrum wings.

A flexible combination of different ways including modification of structural parameters in the first cladding ring, and choice of fluids infiltration leads to the high nonlinearity and ultra-flattened dispersion of proposed PCF. These fibers offer a broader bandwidth with much lower input pulse energy when compared to previous C_7H_8 infiltrated PCF (Hoang et al. 2018; Thi et al. 2022; Van et al. 2017). The proposed designed model can be a new class of fibers for all-fiber SC sources as an alternative to glass core fibers for the next generation of a broadband source.

Acknowledgements This research is funded by Vietnam National Foundation for Science and Technology Development (NAFOSTED) under grant number 103.03-2020.03 and Vietnam's Ministry of Education and Training (B2021-DHH-08).

Funding Vietnam National Foundation for Science and Technology Development (NAFOSTED),103.03-2020.03,Lanh Chu Van,Vietnam's Ministry of Education and Training,B2021-DHH-08,Thuy Nguyen Thi

Data availability No data availability statement.

Declarations

Conflict of interest We declare that the authors do not have any conflicts of interest.

References

Agrawal, G.: Highly nonlinear fibers. In: Nonlinear Fiber Optics, pp. 457–496. Elsevier (2013). https://doi.org/10.1016/B978-0-12-397023-7.00011-5

Ahmad, R., Komanec, M., Zvanovec, S.: Ultra-wideband mid-infrared supercontinuum generation in liquid-filled circular photonic crystal fiber. J. Nanophoton. **14**(2), 026016 (2020)

Alam, Md.Z., Tahmid, Md.I., Mouna, S.T., Islam, Md.A., Alam, M.S.: Design of a novel star type photonic crystal fiber for mid-infrared supercontinuum generation. Opt. Commun. **500**, 127322 (2021)

Begum, F., Namihira, Y., Kinjo, T., Kaijage, S.: Supercontinuum generation in square photonic crystal fiber with nearly zero ultra-flattened chromatic dispersion and fabrication tolerance analysis. Opt. Commun. **284**(4), 965–970 (2011)

Dashtban, Z., Salehi, M.R., Abiri, E.: Supercontinuum generation in near- and mid-infrared spectral region using highly nonlinear silicon-core photonic crystal fiber for sensing applications. Photon. Nanostruct. Fundam. Applic. **46**, 100942 (2021)

Dinh, Q.H., Pniewski, J., Van, H.L., Ramaniuk, A., Long, V.C., Borzycki, K., Xuan, K.D., Klimczak, M., Buczyński, R.: Optimization of optical properties of photonic crystal fibers infiltrated with carbon tetrachloride for supercontinuum generation with subnanojoule femtosecond pulses. Appl. Opt. **57**(14), 3738–3746 (2018)

Dudley, J.M.: Coherence properties of supercontinuum spectra generated in photonic crystal and tapered optical fibers. Opt. Lett. **27**(13), 1180–1182 (2002)

Dudley, J.M., Taylor, J.R.: Supercontinuum Generation in Optical Fibers. Cambridge University Press, Cambridge (2010)

Dudley, J.M., Genty, G., Coen, S.: Supercontinuum generation in photonic crystal fiber. Rev. Modern Phys. **78**(4), 1135–1184 (2006)

Fang, Y., Bao, C., Wang, Z., Liu, B., Zhang, L., Han, X., He, Y., Huang, H., Ren, Y., Pan, Z., Yue, Y.: Three-octave supercontinuum generation using SiO_2 cladded Si_3N_4 slot waveguide with all-normal dispersion. J. Lightwave Technol. **38**(13), 3431–3438 (2020)

Fanjoux, G., Margueron, S., Beugnot, J.C., Sylvestre, T.: Supercontinuum generation by stimulated Raman-Kerr scattering in a liquid-core optical fiber. J. Opt. Soc. Am. B **34**(8), 1677–1683 (2017)

Ferreira, M.F.S.: Introduction. In: Ferreira, M.F.S. (ed.) Optical Signal Processing in Highly Nonlinear Fibers, pp. 1–4. CRC Press, First edition. | Boca Raton, FL : CRC Press, 2020. (2020). https://doi.org/10.1201/9780429262111-1

Finot, C., Kibler, B., Provost, L., Wabnitz, S.: Beneficial impact of wave-breaking for coherent continuum formation in normally dispersive nonlinear fibers. J. Opt. Soc. Am. B **25**(11), 1938–1337 (2008)

Gallazzi, F., Cáceres, I., Monroy, L., Nuño, J., Pulido, C., Corredera, P., Naranjo, F.B., Herráez, M.G., Castañón, J.D.A.: Ultralong ring laser supercontinuum sources using standard telecommunication fibre. Opt. Laser Technol. **147**, 107632 (2022)

Hartl, I., Li, X.D., Chudoba, C., Ghanta, R.K., Ko, T.H., Fujimoto, J.G., Ranka, J.K., Windeler, R.S.: Ultrahigh-resolution optical coherence tomography using continuum generation in an air-silica microstructure optical fiber. Opt. Lett. **26**(9), 608–610 (2001)

Hoang, V.T., Kasztelanic, R., Anuszkiewicz, A., Stepniewski, G., Filipkowski, A., Ertman, S., Pysz, D., Wolinski, T., Xuan, K.D., Klimczak, M., Buczynski, R.: All-normal dispersion supercontinuum generation in photonic crystal fibers with large hollow cores infiltrated with toluene. Opt. Mater. Expr. **8**(11), 3568–3582 (2018)

Hoang, V.T., Kasztelanic, R., Filipkowski, A., Stępniewski, G., Pysz, D., Klimczak, M., Ertman, S., Long, V.C., Woliński, T.R., Trippenbach, M., Xuan, K.D., Śmietana, M., Buczyński, R.: Supercontinuum generation in an all-normal dispersion large core photonic crystal fiber infiltrated with carbon tetrachloride. Opt. Mater. Expr. **9**(5), 2264–2278 (2019)

Hoang, V.T., Kasztelanic, R., Stępniewski, G., Xuan, K.D., Long, V.C., Trippenbach, M., Klimczak, M., Buczyński, R., Pniewski, J.: Femtosecond supercontinuum generation around 1560 nm in hollow-core photonic crystal fibers filled with carbon tetrachloride. Appl. Opt. **59**(12), 3720–3725 (2020)

Hsu, J.M.: Tailoring of nearly zero flattened dispersion photonic crystal fibers. Opt. Commun. **361**, 104–109 (2016)

Huang, C., Liao, M., Bi, W., Li, X., Hu, L., Zhang, L., Wang, L., Qin, G., Xue, T., Chen, D., Gao, W.: Ultraflat, broadband, and highly coherent supercontinuum generation in all-solid microstructured optical fibers with all-normal dispersion. Photon. Res. **6**(6), 601–608 (2018a)

Huang, T., Huang, P., Cheng, Z., Liao, J., Wu, X., Pan, J.: Design and analysis of a hexagonal tellurite photonic crystal fiber with broadband ultra-flattened dispersion in mid-IR. Optik **167**, 144–149 (2018b)

Huang, T., Wei, Q., Wu, Z., Wu, X., Huang, P., Cheng, Z., Shum, P.P.: Ultra-flattened normal dispersion fiber for supercontinuum and dissipative soliton resonance generation at 2 μm. IEEE Photon. J. **11**(3), 7101511 (2019)

Huang, Y., Yang, H., Zhao, S., Mao, Y., Chen, S.: Design of photonic crystal fibers with flat dispersion and three zero dispersion wavelengths for coherent supercontinuum generation in both normal and anomalous regions. Result. Phys. **23**, 104033 (2021)

Islam, Md.S., Sultana, J., Dinovitser, A., Brian, W.HNg., Abbott, D.A.: Novel zeonex basedoligoporous-core photonic crystal fiber for polarization preserving terahertz applications. Opt. Commun. **413**, 242–248 (2018)

Jones, D.J., Diddams, S.A., Ranka, J.K., Stentz, A., Windeler, R.S., Hall, J.L., Cundiff, S.T.: Carrier-envelope phase control of femtosecond mode-locked lasers and direct optical frequency synthesis. Sci. **288**(5466), 635–639 (2000)

Kaminski, C.F., Watt, R.S., Elder, A.D., Frank, J.H., Hult, J.: Supercontinuum radiation for applications in chemical sensing and microscopy. Appl. Phys. B **92**(3), 367–378 (2008)

Kato, T., Suetsugu, Y., Takagi, M., Sasaoka, E., Nishimura, M.: Measurement of the nonlinear refractive index in optical fiber by the cross-phase-modulation method with depolarized pump light. Opt. Lett. **20**(9), 988–990 (1995)

Kedenburg, S., Vieweg, M., Gissibl, T., Giessen, H.: Linear refractive index and absorption measurements of nonlinear optical liquids in the visible and near-infrared spectral region. Opt. Mater. Expr. **2**(11), 1588–1611 (2012)

Knight, J.C.: Photonic. Cryst. Fibre. Nat. **424**(6950), 847–851 (2003)

Kumar, P., Kumar, V., Roy, J.S.: Design of quad core photonic crystal fibers with flattened zero dispersion. Int. J. Electron. Commun. **98**, 265–272 (2019)

Kumar, P., Fiaboe, K.F., Roy, J.S.: Design of nonlinear photonic crystal fibers with ultra-flattened zero dispersion for supercontinuum generation. ETRI J. **42**(2), 282–291 (2020)

Le, H.V., Cao, V.L., Nguyen, H.T., Nguyen, A.M., Buczyński, R., Kasztelanic, R.: Application of ethanol infiltration for ultra-flattened normal dispersion in fused silica photonic crystal fibers. Laser Phys. **28**, 115106 (2018)

Lee, Y.S., Lee, C.G., Bahloul, F., Kim, S., Oh, K.: Simultaneously achieving a large negative dispersion and a high birefringence over Er and Tm dual gain bands in a square lattice photonic crystal fiber. J. Lightwave Technol. **37**(4), 1254–1263 (2019)

Lemière, A., Maldonado, A., Désévédavy, F., Kibler, B., Mathey, P., Gadret, G., Jules, J.C., Hoa, N.P.T., Suzuki, T., Ohishi, Y., Smektala, F.: Towards absorption spectroscopy by means of mid-infrared supercontinuum generation in a step index tellurite fiber. Laser Phys. **31**(2), 025702–025708 (2021)

Ling, W.J., Li, K., Zuo, Y.Y.: Supercontinuum generation in nonperiodic photonic crystal fibers and its application in frequency metrology. Appl. Mechan. Mater. **302**, 194–199 (2013)

Maji, P.S., Chaudhuri, P.R.: Supercontinuum generation in ultra-flat near zero dispersion PCF with selective liquid infiltration. Optik **125**(20), 5986–5992 (2014)

Medjouri, A., Simohamed, L.M., Ziane, O., Boudrioua, A., Becer, Z.: Design of a circular photonic crystal fiber with flattened chromatic dispersion using a defected core and selectively reduced air holes: application to supercontinuum generation at 1.55 μm. Photon. Nanostruct. Fundam. App. **16**, 43–50 (2015)

Medjouri, A., Meraghni, E.B., Hathroubi, H., Abed, D., Simohamed, L.M., Ziane, O.: Design of ZBLAN photonic crystal fiber with nearly zero ultra-flattened chromatic dispersion for supercontinuum generation. Optik **135**, 417–425 (2017)

Medvedkov, O.I., Vasiliev, S.A., Gnusin, P.I., Dianov, E.M.: Photosensitivity of optical fibers with extremely high germanium concentration. Opt. Mater. Expr **2**(11), 1478–1489 (2012)

Mei, C., Wu, Y., Qiu, S., Yuan, J., Zhou, X., Long, K.: Design of dual-core photonic crystal fiber for temperature sensor based on surface plasmon resonance effect. Opt. Commun. **508**, 127838 (2022)

Moutzouris, K., Papamichael, M., Betsis, S.C., Stavrakas, I., Hloupis, G., Triantis, D.: Refractive, dispersive and thermo-optic properties of twelve organic solvents in the visible and near-infrared. Appl. Phys. B **116**, 617–622 (2014)

Pires, H., Baudisch, M., Sanchez, D., Hemmer, M., Biegert, J.: Ultrashort pulse generation in the mid-IR. Prog. Quantum Electron. **43**, 1–30 (2015)

Raei, R., Heidari, M.E., Saghaei, H.: Supercontinuum generation in organic liquid-liquid core-cladding photonic crystal fiber in visible and near-infrared regions. J. Opt. Soc. Am. B **35**(2), 323–330 (2018)

Roy, S., Ghosh, D., Bhadra, S.K., Agrawal, G.P.: Role of dispersion profile in controlling emission of dispersive waves by solitons in supercontinuum generation. Opt. Commun. **283**(15), 3081–3088 (2010)

Saitoh, K., Koshiba, M., Hasegawa, T., Sasaoka, E.: Chromatic dispersion control in photonic crystal fibers: application to ultra-flattened dispersion. Opt. Expr **11**(8), 843–852 (2003)

Saitoh, K., Florous, N.J., Koshiba, M.: Theoretical realization of holey fiber with flat chromatic dispersion and large mode area: an intriguing defected approach. Opt. Lett. **31**(1), 26–28 (2006)

Shang, H., Sun, D., Zhang, M., Song, J., Yang, Z., Liu, D., Zeng, S., Wan, L., Zhang, B., Wang, Z., Li, Z., Liu, Y.G.: On-chip detector based on supercontinuum generation in chalcogenide waveguide. J. Lightwave Technol. **39**(12), 3890–3895 (2021)

Sharafali, A., Ali, A.K.S., Lakshmanan, M.: Modulation instability induced supercontinuum generation in liquid core suspended photonic crystal fiber with cubic-quintic nonlinearities. Phys. Lett. A **399**, 127290 (2021)

Smirnov, S.V., Ania-Castanon, J.D., Ellingham, T.J., Kobtsev, S.M., Kukarin, S., Turitsyn, S.K.: Optical spectral broadening and supercontinuum generation in telecom applications. Opt. Fiber. Technol. **12**(2), 122–147 (2006)

Sobon, G., Sotor, J., Martynkien, T., Abramski, K.M.: Ultra-broadband dissipative soliton and noise-like pulse generation from a normal dispersion mode-locked Tm-doped all-fiber laser. Opt. Expr. **24**, 6156–6161 (2016)

Stępniewski, G., Pniewski, J., Pysz, D., Cimek, J., Stępień, R., Klimczak, M., Buczynski, R.: Development of dispersion-optimized photonic crystal fibers based on heavy metal oxide glasses for broadband infrared supercontinuum generation with fiber lasers. Sens. **18**(12), 4127 (2018)

Sultana, J., Islam, Md.S., Islam, M.R., Abbott, D.: High numerical aperture, highly birefringent novel photonic crystal fiber for medical imaging applications. Electron. Lett. **54**(2), 61–62 (2018)

Tan, C.Z.: Determination of refractive index of silica glass for infrared wavelengths by IR spectroscopy. J. Non-Cryst. Solid. **223**(1–2), 158–163 (1998)

Thévenaz, L.: Advanced Fiber Optics Concept and Technology, 1st edn. EPFL Press, New York (2011)

Thi, T.N., Trong, D.H., Tran, B.T.L., Van, T.D., Van, L.C.: Optimization of optical properties of toluene-core photonic crystal fibers with circle lattice for supercontinuum generation. J. Opt. **51**(3), 678–688 (2022)

Tran, B.T.L., Thi, T.N., Minh, N.V.T., Canh, T.L., Van, M.L., Long, V.C., Xuan, K.D., Van, L.C.: Analysis of dispersion characteristics of solid-core PCFs with different types of lattice in the claddings, infiltrated with ethanol. Photon. Lett. Poland **12**(4), 106–108 (2020)

Van, L.C., Anuszkiewicz, A., Ramaniuk, A., Kasztelanic, R., Xuan, K.D., Long, V.C., Trippenbach, M., Buczyński, R.: Supercontinuum generation in photonic crystal fibers with core filled with toluene. J. Opt. **19**, 125604–125609 (2017)

Van, L.C., Hoang, V.T., Long, V.C., Borzycki, K., Xuan, K.D., Quoc, V.T., Trippenbach, M., Buczyński, R., Pniewski, J.: Optimization of optical properties of photonic crystal fibers infiltrated with chloroform for supercontinuum generation. Laser Phys. **29**(7), 075107 (2019)

Van, L.C., Hoang, V.T., Long, V.C., Borzycki, K., Xuan, K.D., Quoc, V.T., Trippenbach, M., Buczyński, R., Pniewski, J.: Supercontinuum generation in photonic crystal fibers infiltrated with nitrobenzene. Laser Phys. **30**(3), 035105 (2020)

Van, H.L., Hoang, V.T., Canh, T.L., Dinh, Q.H., Nguyen, H.T., Minh, N.V.T., Klimczak, M., Buczynski, R., Kasztelanic, R.: Silica-based photonic crystal fiber infiltrated with 1,2-dibromoethane for supercontinuum generation. Appl. Opt. **60**(24), 7268–7278 (2021)

Van, L.C., Thi, T.N., Tran, B.T.L., Trong, D.H., Minh, N.V.T., Le, H.V., Hoang, V.T.: Multi-octave supercontinuum generation in As_2Se_3 chalcogenide photonic crystal fiber. Photon. Nanostruct. Fundam. Appl. **48**, 100986 (2022)

Vieweg, M., Gissibl, T., Pricking, S., Kuhlmey, B.T., Wu, D.C., Eggleton, B.J., Giessen, H.: Ultrafast nonlinear optofluidics in selectively liquid-filled photonic crystal fibers. Opt. Expr. **18**, 25232–25240 (2010)

Yang, X., Lu, Y., Liu, B., Yao, J.: Fiber ring laser temperature sensor based on liquid-filled photonic crystal fiber. IEEE Sens. J. **17**(12), 6948–6952 (2017)

Yoshii, K., Nomura, J., Taguchi, K., Hisa, i Y., Hong, F.L.: Optical frequency metrology study on nonlinear processes in a waveguide device for ultrabroadband comb generation. Phys. Rev. Appl. **11**, 054031 (2019)
Zeleny, R., Lucki, M.: Nearly zero dispersion-flattened photonic crystal fiber with fluorine-doped threefold symmetry core. Opt. Eng. **52**(4), 045003 (2013)